Geophysical Journal International

Geophys. J. Int. (2013) **194,** 1554–1558
Advance Access publication 2013 June 26

doi: 10.1093/gji/ggt201

EXPRESS LETTER

Experimental characterization of strain localization in rock

Hao Zhang, Ganyun Huang, Haipeng Song and Yilan Kang

Tianjin Key Laboratory of Modern Engineering Mechanics, School of Mechanical Engineering, Tianjin University, Tianjin 300072*, People's Republic of China. E-mail: tju_ylkang@tju.edu.cn*

Accepted 2013 May 15. Received 2013 May 14; in original form 2013 April 5

SUMMARY

In this study, damage evolution and strain localization in sandstone have been experimentally investigated in uniaxial compression tests. A digital image correlation technique has been applied to obtain apparent strain fields which can visually display the deformation and damage evolution of rock. The experimental results show that regions with apparent strain concentration (RASC) develop at the initial loading stage and distribute diffusely on the sample surface which may correspond to the damaged areas. With incremental load, the RASCs localize spatially, probably via coalescence into a line-shaped area that behaves like a macroscopic crack leading to the eventual failure of the specimen. A factor D_{RASC} representing the deviation of the average apparent strain in RASCs from the average on the whole sample surface and a localization factor L_{f}, are proposed to characterize the evolution of damage and localization. D_{RASC} increases slowly in the initial phase of loading and rises rapidly after the onset of localization. L_{f} decreases during loading which indicate the localization of spatial distribution of damage. The two factors can be used to well reflect the damage evolution and strain localization of rock specimens under compression.

Key words: Image processing; Fractures and faults; High strain deformation zones; Mechanics, theory, and modelling.

GJI Seismology

1 INTRODUCTION

The understanding of damage and failure mechanisms of geomaterials (soils, concrete, rocks, etc.) under compression is an important basis for seismological and geodynamical studies. The macroscopic deformation and failure of rock is a gradual process of damage accumulation, crack initiation, propagation, interaction and eventual failure (Amitrano 2006). Usually, failure is accompanied by localization of deformation and the damage zone (Paliwal & Ramesh 2008; Svahnberg & Piazolo 2010). Indeed, strain localization under compression occurs almost unequivocally in geomaterials ranging from small laboratory specimens (Louis *et al.* 2007; Charalampidou *et al.* 2011) to exhumed fault zones in the field (Eichhubl *et al.* 2010). The localization of damage and strain can influence the stress distribution and weaken the mechanical performance of the rock (Lockner *et al.* 1991; Besuelle *et al.* 2000). Thus, understanding the mechanisms and evolution of damage or strain localization in rocks has attracted numerous research efforts. Baud *et al.* observed that the compaction localization can be associated with stress states in the transitional regime from brittle faulting to cataclastic flow in porous sandstones (Baud *et al.* 2004). Svahnberg and Piazolo inferred that strain localization in plagioclase-rich rocks was caused by recrystallization and the development of a crystallographic preferred orientation (CPO) in continuous recrystallized bands (Svahnberg & Piazolo 2010).

While mechanisms of localization have been proposed and probed, how the localization results in eventual failure has received much less attention, which motivates us to conduct the present work. To this end, full-field measurements for displacement and strain are desirable to capture the evolution of localization. Specific techniques referred to as full-field measurements have been developed to provide the deformation history and the eventual development of localization and damage of laboratory specimens (Lenoir *et al.* 2007). Kozicki and Tejchman investigated the strain localization in concrete using digital image correlation (DIC) technique (Kozicki & Tejchman 2007). Hall *et al.* identified the characteristic features of the localized band in granular material (Hall *et al.* 2010), and localized deformation in porous carbonate was also discovered by multiscale DIC (Dautriat *et al.* 2011). Hao *et al.* (2010) defined fluctuations of strains, and Ma & Zhou (2008) used the standard deviation of the maximum shear strain field to describe the damage evolution of rock. Katz & Reches (2004) experimentally analysed the evolution of stress-induced damage and the eventual brittle failure of Mount Scott granite. Girard *et al.* used spatial correlation integral to numerically investigate the progressive damage localization (Girard *et al.* 2010). Accelerating evolution of damage localization is closely related to the catastrophic failure of rock, however, scientific descriptions of damage evolution, especially experimental characterizations of the spatial distribution of damage are few.

This paper is concerned with the characterization of strain localization in sandstone subjected to uniaxial compression. The experimental results show the evolution of damage, strain localization, crack propagation and failure in rock. Through the analysis of apparent strain fields, two parameters are presented that reflect the degree of strain concentration and the degree of localization of its spatial distribution, respectively. The evolution of these parameters in the experiment is presented and discussed.

2 EXPERIMENTAL MATERIAL AND METHODOLOGY

Uniaxial compression tests were conducted on prismatic Yunnan sandstone specimens of dimension 25 × 25 × 50 mm. A compression load device (CSS-44100) is used in the axial compression condition, with crosshead displacement control at a constant velocity of 1 μm s^{-1} up to failure of the sample. One surface of the rock sample was sprayed with random black and white artificial speckle and photographs of the surface were taken throughout the loading with a Basler A202k charged couple discharge (CCD) camera. The resolution of the camera was 1004 × 1003 pixels and the images with length-pixel ratio of 60.8 μm $pixel^{-1}$ were continually acquired at rate was 1 fps (frame per second).

DIC analysis can thus be carried out on the acquired images to yield fields of displacement and hence apparent strain fields over the observed surface. DIC is widely used for displacement and strain field measurements due to its characteristics of non-contact, real time, wide measuring range and simple optical setup, etc. (Kang *et al.* 2005; Pan *et al.* 2009). Previously, Zhang *et al.* (2012) and Ma *et al.* (2011) have applied this technique to investigate the failure in rock samples. Walter (2011) applied this technique to monitor volcano deformation, which demonstrated the validity of DIC on rock laboratory tests and geological observations.

After acquisition of the images at different stages of deformation, the displacement field in the DIC calculation area can be computed by tracing the grey level value of each point in the reference and deformed images and performing their image correlation. The correlation coefficient in that process is defined as follows:

$$C(X) = \frac{\sum_{i=1}^{m}\sum_{j=1}^{m}\left[f(x_i, y_j) - \bar{f}\right]\cdot\left[g(x_i^*, y_j^*) - \bar{g}\right]}{\sqrt{\sum_{i=1}^{m}\sum_{j=1}^{m}\left[f(x_i, y_j) - \bar{f}\right]^2 \cdot \sum_{i=1}^{m}\sum_{j=1}^{m}\left[g(x_i^*, y_j^*) - \bar{g}\right]^2}} \tag{1}$$

$$x^* = x + u + \frac{\partial u}{\partial x}\Delta x + \frac{\partial u}{\partial y}\Delta y$$

$$y^* = y + v + \frac{\partial v}{\partial x}\Delta x + \frac{\partial v}{\partial y}\Delta y \tag{2}$$

where $X = \left(u, v, \partial u/\partial x, \partial u/\partial y, \partial v/\partial x, \partial v/\partial y\right)$ containing six deformation parameters, $f(x, y)$ is the grey level value at coordinate (x, y) for the reference image and $g(x^*, y^*)$ the grey level value at coordinate (x^*, y^*) for the target image, $\bar{f}$ and $\bar{g}$ the average grey values of the image $f(x, y)$ and $g(x^*, y^*)$, respectively. A calculation subset size (21 × 21 pixels) and step length (10 pixels) were chosen to increase the spatial resolution of measurement. From this matching process the displacement of each gridpoint can be determined. The displacement measurement accuracy in our test was at least 1 μm based on the calibration work conducted in the same experimental condition. The strain field can be calculated based on displacement components by geometrical relations.

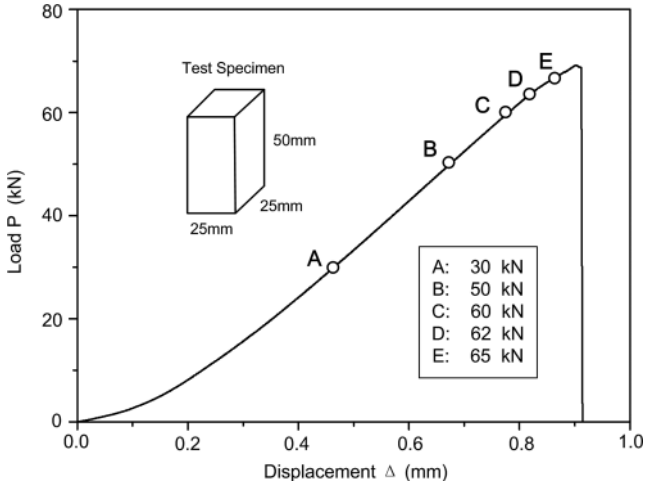

Figure 1. Load–displacement curve in uniaxial compression test.

3 EXPERIMENTAL RESULTS AND DISSCUSION

Fig. 1 shows the evolution of the differential load P with respect to the axial displacement during the uniaxial compression test. After an initial slow increment, the relation between the load and displacement is virtually linear for most of the curve. When the load amounts to about 69 kN at a displacement value of 0.91 mm or so, the load suddenly drops which is associated with the eventual failure of the specimen. Thus, the compression behaviour of our sandstone samples is common to the brittle materials. Since via DIC technique, the displacement field on the samples' surfaces can be obtained and hence the strain field, we have chosen points A to E indicated in Fig. 1 for such analysis. It is worth mentioning that the strain here should be understood as an apparent one which actually reflects the displacement gradient when crack develops. Fig. 2 presents the evolution of the apparent principal strain ε_1 fields. It can be found that at a load level of $P = 30$ kN, distributed regions of larger than average ε_1 can be observed scattered or discretely over the surface (Fig. 2a). These regions will be referred to as regions of apparent strain concentration (RASCs) that may represent the damaged area. With further loading, the RASCs at the top right and left bottom corners of the specimen respectively join up and spatially become somewhat continuous (Fig. 2b). The RASCs evolve into a localization band of belt-shape along the diagonal of the specimen (Fig. 2c) when the axial load reaches about 60 kN. With another increment of load, regions with largest apparent strain are distributed at the middle of the diagonal, which corresponds to a macroscopic crack initiation in the localization band shown in Fig. 2(d). As can be seen in Fig. 2(e), the damaged regions coalescence further and a macroscopic crack propagates towards the top and bottom of the specimen, leading to eventual failure. Therefore, the failure of the sandstone results from the coalescence of distributed damage that locally develops.

Given the appearance of the RASCs, we have singled out the regions with ε_1 in the range of top largest values at each loading level and as shown in Fig. 3 for top 7.5 per cent, they can well reflect the strain distribution pattern in Fig. 2. We will use this method to select the RASCs for an analysis of the damage evolution. As

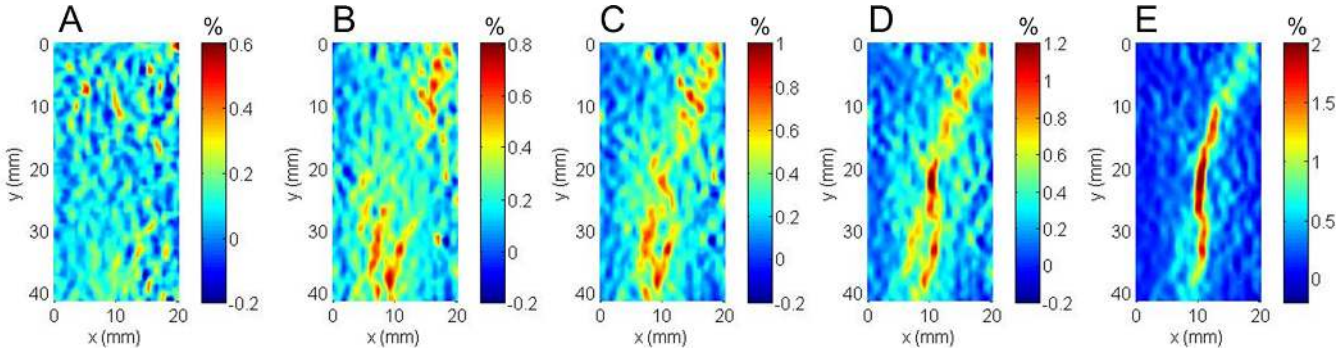

Figure 2. Apparent principal strain ε_1 fields at five levels of stress referred to as A to E on the load–displacement curve presented in Fig. 1.

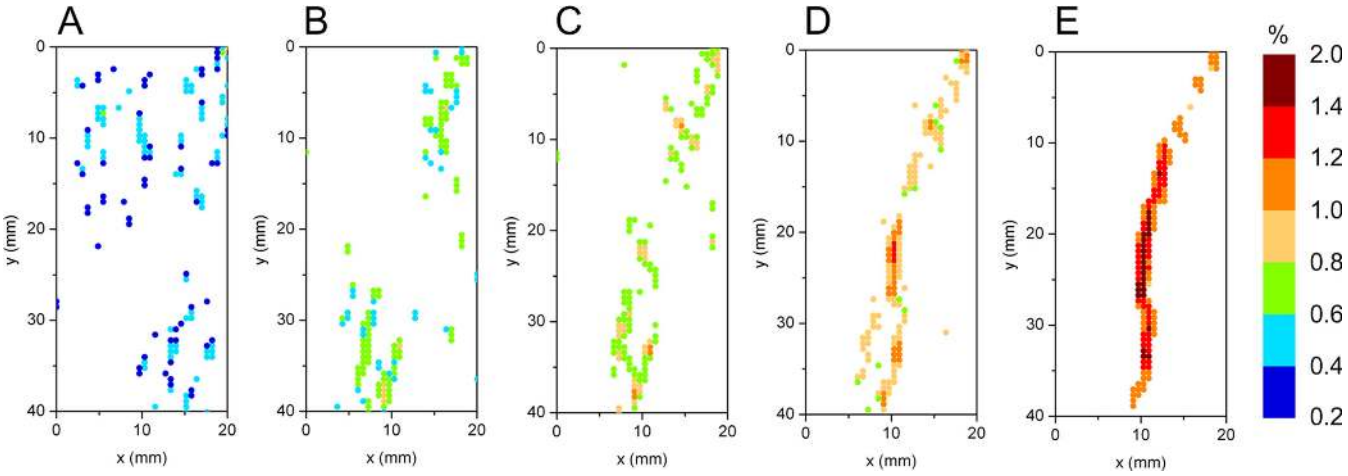

Figure 3. Spatial distribution of top 7.5 per cent apparent strain points.

indicated above the damage evolution with loading involves spatial localization and the increment of apparent strain concentration, so at least two parameters are necessary for their characterization. To this end, we introduce

$$L_{\mathrm{f}} = 1 - C_{xy} \tag{3}$$

and

$$D_{\mathrm{RASC}} = \bar{\varepsilon}_n \big/ \bar{\varepsilon}_{\max} \tag{4}$$

with

$$C_{xy} = \frac{s_{xy}}{s_x s_y} = \frac{\sum_{j=1}^{n} \left(x_j - \bar{x}\right)\left(y_j - \bar{y}\right)}{\sqrt{\sum_{j=1}^{n} \left(x_j - \bar{x}\right)^2} \sqrt{\sum_{j=1}^{n} \left(y_j - \bar{y}\right)^2}} \tag{5}$$

$$\bar{\varepsilon}_n = \frac{1}{n} \sum_{i=1}^{n} \varepsilon_1^i - \frac{1}{N} \sum_{i=1}^{N} \varepsilon_1^i. \tag{6}$$

In eq. (5), C_{xy} is the correlation coefficient; s_x, s_y and s_{xy} are the standard deviations and the covariance; n is the number of the selected points with x_j and y_j being their coordinates and, $\bar{x}$ and $\bar{y}$ the average values of $\{x_j\}$ and $\{y_j\}$. Thus, L_{f} represents a measure of the linearity of the localized deformation. In eq. (6), ε_1^i is apparent principle strain at point i, N is the total number of data points in the field and $\bar{\varepsilon}_{\max}$ corresponds to the value of $\bar{\varepsilon}_n$ at peak load. It can then be easily seen that D_{RASC} is the deviation of the strain average in RASCs from the overall strain average on the surface and can be used to characterize the average strain concentration in RASCs.

Figs 4(a) and (b), respectively demonstrate the effect of different top percentage values of the selected points with strain concentration on the behaviour of the damage localization factor L_{f} and D_{RASC}. Evidently, that effect is trivial. It is interesting to note that L_{f} decreases steadily with load and the slope becomes increasingly sharp with load. More specifically, L_{f} is greater than 0.7 before point A (Fig. 4a), due to the scattered distribution of the RASCs. Corresponding to the process of strain localization, it then decreases sharply from A to C. The value is less than 0.2 after the formation of the macroscopic crack (point D). So the evolution of scattered damage into a localized macroscopic crack can be roughly read from the L_{f} versus load curve. However, at what load level the macroscopic crack forms is not obvious. Instead, as shown in Fig. 4(b), the factor D_{RASC} initially increases very slowly with loading. When the applied load approaches the peak load, it rises very rapidly and suddenly, which corresponds to the formation of the macroscopic crack since it induces a large displacement gradient across the crack faces and hence large apparent strain. The relation between D_{RASC} and the applied load seems to obey a percolation threshold model. Thus, we use $D_{\mathrm{RASC}}(P) = |P - P_{\mathrm{c}}|^{-\alpha}$ where P_{c} is percolation threshold and α stands for critical exponent, to fit the experimental results in Fig. 4(b). It can be obtained that the fitting parameters $P_{\mathrm{c}} = 66.557$, $\alpha = 0.541$ for sandstones in the tests. So the critical load for the formation of a macroscopic crack might be estimated by the percolation threshold. Appearance of the percolation-like evolution of the factor D_{RASC} is not surprising. As mentioned earlier, the eventual failure in the present experiments is the result of

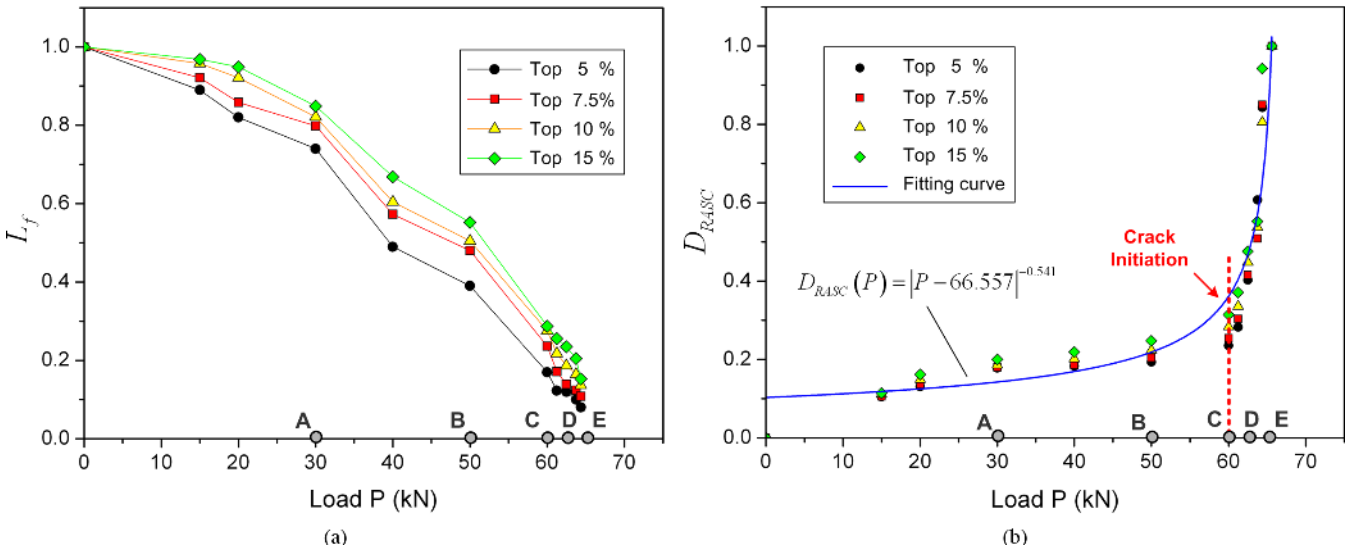

Figure 4. Variation of L_f and D_{RASC} with increment of load. (a) Localization factor L_f. (b) The factor D_{RASC} of RASCs using different top percentages of selected apparent strain ε_1 points.

coalescence of distributed damages that developed locally. It is known physically that such a process can be described by a percolation model where a critical damage density may be the threshold. Since the damage density can be correlated with the applied load and D_{RASC} indeed represents the apparent strain concentration at large damage clusters, it is natural to follow the above mentioned scaling between D_{RASC} and the applied load. Based on such arguments, it is anticipated that provided the brittle materials fail through coalescence of distributed damage, D_{RASC} can be defined with the percolation like evolution with the applied load, although further experiments are necessary to verify it.

4 CONCLUSIONS

In this work, uniaxial compression tests were conducted to investigate the damage and failure process of rock by DIC technique. The apparent strain analysis reveals the pattern of strain localization during loading, and then subsequent initiation of the crack inside the localized region resulting in failure of rock. A localization factor L_f and a strain concentration factor D_{RASC}, are presented and combined to quantitatively describe the localization of the damage distribution and the level of rock damage. Variations of L_f and D_{RASC} during the loading process are given, which can experimentally well characterize the evolution of diffuse damage, strain localization, crack initiation and failure in rock.

ACKNOWLEDGEMENTS

This work was supported by the National Natural Science Foundation of China (NSFC, Grant No.11127202, No.11072170 and No.11272232).

REFERENCES

Amitrano, D., 2006. Rupture by damage accumulation in rocks, *Int. J. Fract.,* **139,** 369–381.

Baud, P., Klein, E. & Wong, T.-F., 2004. Compaction localization in porous sandstones: spatial evolution of damage and acoustic emission activity, *J. Struct. Geol.,* **26,** 603–624.

Besuelle, P., Desrues, J. & Raynaud, S., 2000. Experimental characterisation of the localisation phenomenon inside a Vosges sandstone in a triaxial cell, *Int. J. Rock. Mech. Min. Sci.,* **37,** 1223–1237.

Charalampidou, E.-M., Hall, S.A., Stanchits, S., Lewis, H. & Viggiani, G., 2011. Characterization of shear and compaction bands in a porous sandstone deformed under triaxial compression, *Tectonophysics,* **503,** 8–17.

Dautriat, J., Bornert, M., Gland, N., Dimanov, A. & Raphanel, J., 2011. Localized deformation induced by heterogeneities in porous carbonate analysed by multi-scale digital image correlation, *Tectonophysics,* **503,** 100–116.

Eichhubl, P., Hooker, J.N. & Laubach, S.E., 2010. Pure and shear-enhanced compaction bands in Aztecsandstone, *J. Struct. Geol.,* **32,** 1873–1886.

Girard, L., Amitrano, D. & Weiss, J., 2010. Failure as a critical phenomenon in a progressive damage model, *J. Stat. Mech. Theory. Exp.,* **2010,** P01013, doi:10.1088/1742-5468/2010/01/P01013.

Hall, S., Muir Wood, D., Ibraim, E. & Viggiani, G., 2010. Localised deformation patterning in 2D granular materials revealed by digital image correlation, *Granul. Matter,* **12,** 1–14.

Hao, S.-W., Xia, M.-F., Ke, F.-J. & Bai, Y.-L., 2010. Evolution of localized damage zone in heterogeneous media, *Int. J. Damage Mech.,* **19,** 787–804.

Kang, Y.-L., Zhang, Z.-F., Wang, H.-W. & Qin, Q.-H., 2005. Experimental investigations of the effect of thickness on fracture toughness of metallic foils, *Mater. Sci. Eng.: A,* **394,** 312–319.

Katz, O. & Reches, Z.E., 2004. Microfracturing, damage, and failure of brittle granites, *J. geophys. Res.,* **109,** doi:10.1029/2002JB001961.

Kozicki, J. & Tejchman, J., 2007. Experimental investigations of strain localization in concrete using digital image correlation (DIC) technique, *Arch. Hydro-Eng. Environ. Mech.,* **54,** 3–24.

Lenoir, N., Bornert, M., Desrues, J., Bésuelle, P. & Viggiani, G., 2007. volumetric digital image correlation applied to X-ray microtomography images from triaxial compression tests on argillaceous rock, *Strain,* **43,** 193–205.

Lockner, D.A., Byerlee, J.D., Kuksenko, V., Ponomarev, A. & Sidorin, A., 1991. Quasi-static fault growth and shear fracture energy in granite, *Nature,* **350,** 39–42.

Louis, L., Wong, T.-F. & Baud, P., 2007. Imaging strain localization by X-ray radiography and digital image correlation: deformation bands in Rothbach sandstone, *J. Struct. Geol.,* **29,** 129–140.

Ma, S.P. & Zhou, H., 2008. Surface strain field evolution of rock specimen during failure process, *Chin. J. Rock Mech. Eng.,* **27,** 1667–1673

Ma, S.P., Yan, D., Wang, X. & Cao, Y.Y., 2011. Damage observation and analysis of a rock Brazilian disc using high-speed DIC method, *Appl. Mech. Mater.,* **70,** 87–92.

Paliwal, B. & Ramesh, K.T., 2008. An interacting micro-crack damage model for failure of brittle materials under compression, *J. Mech. Phys. Solid.,* **56,** 896–923.

Pan, B., Qian, K., Xie, H. & Asundi, A., 2009. Two-dimensional digital image correlation for in-plane displacement and strain measurement: a review, *Meas. Sci. Technol.,* **20,** 062001.

Svahnberg, H. & Piazolo, S., 2010. The initiation of strain localisation in plagioclase-rich rocks: insights from detailed microstructural analyses, *J. Struct. Geol.,* **32,** 1404–1416.

Walter, T.R., 2011. Low cost volcano deformation monitoring: optical strain measurement and application to Mount St. Helens data, *Geophys. J. Int.*, **186,** 699–705.

Zhang, H., Huang, G., Song, H. & Kang, Y., 2012. Experimental investigation of deformation and failure mechanisms in rock under indentation by digital image correlation, *Eng. Fract. Mech.,* **96,** 667–675.